Journal of Solid Mechanics Vol. 15, No. 3 (2023) pp. 274-287
DOI: 10.22034/jsm.2023.1970881.1754

Research Paper

Improvement of the Extended-Enriched MLPG Meshless Method by Using Optimal Nodal Points Distribution to Find 3D-SIFs

B. Ariannezhad [1], Sh. Shahrooi [1,*], M. Shishehsaz [2]

[1] *Department of Mechanical Engineering, Ahvaz Branch, Islamic Azad University, Ahvaz, Iran*
[2] *Department of Mechanical Engineering, Shahid Chamran University, Ahvaz, Iran*

Received 28 May 2023; accepted 2 July 2023

ABSTRACT

Using appropriate shape functions and distribution of nodal points in local domains and sub-domains and choosing an approximation or interpolation method has an effective role in the application of meshless methods for the analysis of computational fracture mechanics problems, especially problems with geometric discontinuity and cracks. In this research, computational geometry technique based on Voronoi diagram and Delaunay triangulation is used to distribute nodal points in the sub-domain of analysis. Therefore, with this technique, the nodal points used in the MLS approximation to apply the MLPG method with enriched polynomial base functions are optimally increased in different steps. By doing this process, the problems caused by too closeness of nodal points in computationally sensitive areas that exist in general methods of nodal point distribution are also solved. Comparing the effect of the number of sentences of basic functions and their order in the definition of shape functions, performing the Mono-objective PSO algorithm to find the penalty factor the coefficient, convergence, arrangement of nodal points during the three stages of Voronoi diagram implementation and the accuracy of the answers found indicates, the efficiency of V-E-MLPG method with N_s=7 and $\beta = 0.0075$ to estimation of 3D-SIFs in computational fracture mechanics.

Keywords : Meshless method; 3D-extend-enriched base functions; Computational geometry; Optimal nodal point distribution; Mono-objective PSO.

1 INTRODUCTION

FOR the mathematical simulation of any physical phenomenon, Partial Differential Equations (PDEs) governing it must be determined. Usually, many problems and phenomena are geometrically complex, there is no analytical solution for them. Therefore, simplifying assumptions or numerical solutions are used to solve them. In numerical

*Corresponding author. Tel.: +98 9039862060; Fax: +98 061 3329200.
E-mail address: shahramshahrooi@iauahvaz.ac.ir (Sh.Shahrooi)

methods, variable fields are calculated using different methods of approximation or interpolation [1]. In addition to applied numerical methods such as the Finite Element Method (FEM), Finite Difference Method (FDM), Finite Volume and the Boundary Element other numerical methods have been introduced to analyze solid mechanics problems, among which the meshless method can be mentioned [2]. These methods, which is introduced by different names, has shown its effectiveness in analyzing moving boundary problems, problems with large deformation and crack growth. Many studies have been conducted using these methods in various topics and fields of mechanical engineering [3-9]. To solve and discretize PDEs, if strong solution is used, because there is no need to integrate and calculate nodal integral equations, the computational cost of this method is reduced compared to the Element Free Galerkin(EFG) method, Meshless Local Petrov-Galerkin (MLPG), Point Interpolation Method (PIM) and Radial Point Interpolation Method (RPIM)[10-12]. Another difference that can be expressed in the applying of meshless methods, are the method of discretization of the equations governing the analysis, the type of base functions for generating shape functions and weight function, using background cells to distribute nodal points, regular or irregular distribution of nodal points in domain analysis and the selection of a suitable method for approximation or interpolation [13-20]. Shape functions are interpolation functions that calculate the value of the field variables at any point of the analysis domain, in terms of the values of nodal points. In fact, shape functions play an important role in the relationship between the known values of variables field and the unknown values at arbitrary points in domain [21]. There are different methods to find shape functions such as: Lagrange's method, Direct method, Superposition Principle method, Lines Product method, Maximum Entropy, Radial Base Function, Moving Kriging, Collocation Discrete Least Square method and Moving or Mixed Discrete Least Square method (MLS and MDLS). But the common feature of these methods is the production of shape functions that have; convergence in solution, compatibility condition, differentiability from the order of *m* or *m-complete* condition and possessing the Dirac Delta property [22-25].Therefore, the selection of Basic Functions(BFs) and their combination, the correct selection of the values of the existing shape parameters in some meshless methods, discretization and appropriate distribution of nodal points in the domains are very important in the production of shape functions[26-33].

In this research, to improve the accuracy of calculations in MLPG method with MLS approximation, mono-objective Particle Swarm Optimization (PSO) algorithm to find the Penalty Factor Coefficient and Voronoi Diagram (VD) has been used to optimally distribute nodal points in sub-domains. Before each step of drawing new cells of the VD in domain analysis, calculations based on nodal data are performed and the error is checked. In the cells with more errors, the nodal points are again increased by running the VD. This operation prevents from increasing the size of the matrix of unknown coefficients and the cost of their calculations. Comparing the results of MLPG method to calculate the 3D-Stress Intensity Factors(3D-SIFs) in cracked shaft under Uni-axial cyclic loading, after three steps of the VD in Extended-Enriched MLPG method (V-E-MLPG) implementation, it led to an increase in the accuracy of calculations. Finally, It will be studied the effect of increasing Linear and Second-order Polynomial Base Functions (PBFs) sentences extracted from the Khayyam-Pascal's pyramid in the definition of Enriched-PBFs (E-PBFs) to produce Shape Functions in V-E-MLPG method.

2 THE MLPG MESHLESS METHOD WITH MOVING LEAST SQUARE (MLS)

The Meshless Local Petrov-Galerkin method (MLPG) with Moving Least Square (MLS) can be used to discretize the Weak-form of partial derivative differential equations. In MLS approximation, displacement values of the nodes are estimated by summation of the Least Square of the discrete time steps. The approximated displacement function by is estimated by the following relation:

$$u^h(x) = \sum_{i=1}^{l} p_i(x)a_i(x) = \mathbf{p}^T(x)\mathbf{a}(x) \qquad \forall x \in \Omega \tag{1}$$

In this equation, " $u^h(x)$ " , "$\mathbf{a}_i(x)$" are the approximated value of " $u(x)$ " and the vector of unknown coefficients respectively. The vector of Polynomial Base Functions (PBFs) which is selected based on the "m^{th} " order polynomial from Khayyam-Pascal's pyramid consists are :

$$\begin{aligned} &\text{Linear Monomial:} \quad \mathbf{p}^T(x)=\begin{bmatrix}1 & x & y & z\end{bmatrix} \qquad N_s=4,\ m=1 \\ &\text{Quadratic:} \quad \mathbf{p}^T(x)=\begin{bmatrix}1 & x & y & z & x^2 & y^2 & z^2 & xy & xz & yz\end{bmatrix} \quad N_s=7,\ m=2 \end{aligned} \tag{2}$$

Quadratic: $\mathbf{p}^{T}(x)=\left[1\ x\ y\ z\ x^2\ y^2\ z^2\ xy\ xz\ yz\right]$ $N_s=10$, $m=2$

Additionally, to find the best coefficients " $\mathbf{a}_i(x)$ " , first it will be defined vector " $\mathbf{J}(x_i)$ " as;

$$\mathbf{J}(x_i)=\sum_{i=1}^{l} w_i(x_i)\left[\mathbf{p}^{T}(x_i)\mathbf{a}(x)-u_i\right]^2 \tag{3}$$

Now, by minimizing the relation (3), in order to approach the approximated value to the actual values can be weitten as follows:

$$\frac{\partial \mathbf{J}}{\partial \mathbf{a}}=0 \tag{4}$$

Solving the resulting system of linear equations, the unknown coefficients are obtained. In Eq.(3), "u_i" stands for the unknown displacement value of the "i^{th}" node and "$W_i(x_i)$"is the weighting functions in MLS approximation which are considered in terms of exponential functions as;

$$w_i(x_i)=\exp\left[-\left(\frac{d}{\alpha_c r_{ei}}\right)^2\right] \qquad i=1,2,3,...,L, \qquad 0\le d\le r_i,\ r_{ei}=\|x-x_i\| \tag{5}$$

where "r_{ei}" corresponds to the i^{th} radius of influence of the domain for nodal points approximation [33]. Sometimes,the weight function is defined based on cubic-spline weights function:

$$w_i(d)=\begin{cases}\frac{2}{3}-4d^2+4d^3 & for\ d\le\frac{1}{2}\\ \frac{4}{3}-4d+4d^2-\frac{4}{3}d^3 & for\ \frac{1}{2}<d\le 1\\ 0 & for\ d>1\end{cases} \tag{6}$$

where in: $d=\frac{r_{ei}}{d_m}$.

In relation(6), "d_m" is the radius effect of the nodal point. The linear relationship between the unknown displacement values "u_i" and the approximated displacement values of "u^h" are calculated based on the following expression:

$$u^h(x)=\sum_{i=1}^{l}\mathbf{\Phi}_i(x)u_i \tag{7}$$

where in the shape functions " $\mathbf{\Phi}_i$ " are calculated based on the following expression:

$$\mathbf{\Phi}_i(x)=\sum_{i=1}^{l}\mathbf{p}_j(x_i)\left[\mathbf{A}_i^{-1}(x)\mathbf{Q}(x_i)\right]_{ij}=\mathbf{p}^{T}(x)(\mathbf{A}^{-1}(x)\mathbf{Q}(x))_i \tag{8}$$

where;

$$\mathbf{A}_i(x)=\sum_{i=1}^{l}w_i(x)\mathbf{p}(x_i)\mathbf{p}^{T}(x_i)=\sum_{i=1}^{l}\mathbf{Q}_i(x_i)\mathbf{p}^{T}(x_i) \tag{9}$$

In problems with field singularity, to eliminate this singularity, one can use the Extended-Enriched Base Functions (E-BFs) or " $\mathbf{p}^{*T}(x)$ " which are selected as the following.

$$\mathbf{p}^{*T}(x)=\mathbf{p}^{T}(x)+\left\{\sqrt{r}\cos\frac{\theta}{2}\quad\sqrt{r}\sin\frac{\theta}{2}\quad\sqrt{r}\sin\frac{\theta}{2}\sin\theta\quad\sqrt{r}\cos\frac{\theta}{2}\sin\theta\right\} \tag{10}$$

Here, "r" stands for the radial distance of each node from the point which its surrounding field is singularized [35].

3 APPLICATION OF MLPG TO 3D-LINEAR ELASTIC PROBLEMS

In three-dimensional solid mechanic problems for a general domain "Ω" with general boundary "Γ", the equilibrium equations and natural and essential boundary conditions are written as:

$$\begin{aligned}&\sigma_{ij,j}+b_i+0 \quad \text{in } \Omega\\ &\sigma_{ij}\overline{n_J}=\overline{t_I} \quad \text{on } \Gamma_t\\ &u_i=\overline{u_I} \quad \text{on } \Gamma_u\end{aligned} \tag{11}$$

where " σ_{ij} " are the stress components, " b_i " are the body force components, " $\overline{t_I}$ " are the surface tractions on the natural boundary, " $\overline{u_I}$ " are the displacement on the essential boundary, " $\overline{n_J}$ " are the normal perpendiculars vector on the natural boundary, " Γ_t " is the natural boundary, and " Γ_u " is the basic boundary. The weak form of the equilibrium equation which is obtained for each node containing Local domain " Ω_q " and local boundary " Γ_q ". By the residue integral method is:

$$\int_{\Omega q} w_I(\sigma_{ij,j}+b_i)d\Omega=0 \tag{12}$$

Using integration by parts and neglecting the body forces, the discrete equations for each nodal point is;

$$\int_{\Omega q} w_I\sigma_{ij,j}d\Omega-\int_{\Gamma_i} w_I\sigma_{ij}\overline{n_J}d\Gamma=0 \tag{13}$$

Now, we are ready to apply the natural boundary conditions. For this purpose, one must realize that if the surface of local volume crosses the geometric boundary surface, then the equations can hardly satisfy the boundary conditions. Therefore, for application of the essential boundary conditions, using the benefit of penalty factors, Eq.(13) is modified with an additional surface integral term which is introduced in Eq. (14).

$$\int_{\Omega q} w_I\sigma_{ij,j}d\Omega-\int_{\Gamma_i} w_I\sigma_{ij}\overline{n_J}d\Gamma-\alpha_p\int_{\Gamma_{qu_i}} w_I(u_i-\overline{u_I})d\Gamma=0 \tag{14}$$

In this equation, " α_p " is the Penalty Factor which is selected by the trial and error in modeling and arrangement of the nodes ($\alpha_p=\beta\frac{E}{D}$, and $\beta\cong 0.01\sim 0.0001$). In this study, to get more accurate results by running the Mono-objective PSO algorithm. If Eq. (14) is discretized and solved based on the displacement fields, and if the approximate displacement function is defined based on shape functions Eq. (8), then, the stress matrix is equal to;

$$\boldsymbol{\sigma}=\mathbf{D}\boldsymbol{\varepsilon}=\mathbf{D}(\mathbf{L}u^h)=\mathbf{DL}(\boldsymbol{\Phi}u)=\mathbf{B}u \tag{15}$$

In Eq. (15), "**L**" , "**D**" and "**B**" are, the differential operator matrix, the matrix of material properties and the strain matrices ($\mathbf{B} = \mathbf{DL\Phi}$). Moreover, the traction vector is written as;

$$\bar{t} = \begin{Bmatrix} t_x \\ t_y \\ t_z \end{Bmatrix} = \bar{n}\mathbf{DB}u \tag{16}$$

Substituting for the traction forces and stress values, the weighting functions " w_I "and their derivatives " w_I^T " in Eq.(14), the stiffness matrix " k_i " and the force vector " $(\mathbf{f})_i$ " for each node are equal to:

$$(\mathbf{k})_i = \int_{\Omega q} w_{,I}^T \mathbf{DB} d\Omega - \int_{\Gamma q_i} w_I^T \bar{n}\mathbf{DB} d\Gamma - \int_{\Gamma qu} w_I^T \bar{n}\mathbf{DB} d\Gamma + \alpha_p \int_{\Gamma_{qu}} w_I^T \mathbf{\Phi} d\Gamma \tag{17}$$

$$(\mathbf{f})_i = \int_{\Gamma qt} w_I^T \bar{t} d\Gamma + \int_{\Gamma qu} w_I^T \mathbf{b} d\Omega + \alpha_p \int_{\Gamma_{qu}} w_I^T \bar{u} d\Gamma \tag{18}$$

In the above relations, "Γ_{qi} ", "Γ_{qt} "and "Γ_{qu} " are, un-subscriber section of Γ_q with Γ, subscriber section of Γ_q with Γ_u and the conterminous section of Γ_t and Γ_u, respectively. Superimposing the stiffness and force matrices to get the global equations $\mathbf{K}^* \mathbf{U}^* = \mathbf{F}^*$, the unknown global displacements are obtained according to the reduced matrix Eq. (19).

$$\mathbf{U} = \mathbf{K}^{-1}\mathbf{F} \tag{19}$$

4 VORONOI DIAGRAM AND REGIONALIZATION OF DOMAIN ANALYSIS TO DISTRIBUTE NODAL POINTS

Interpolation means finding the values of the function at the points where the value of the function is known in the neighborhood of those points. The choice of points, density and distribution of nodal points, the influence domain and the radius of its, as well as the selection of the appropriate interpolation method, play an important role in the accuracy of calculations.

The Voronoi Diagrams (VD), by receiving a set of points, divide the space (analysis domain) based on the closest point to the desired points. Each of the divided areas is called a cell (cell P_i). In each cell there is a point where the value of the function at that point must be interpolated based on the known values of the other points. The selection of the other points within the cell follows the rule of the closest distance to the desired point (Nearest-Neighbor Interpolation). Therefore, this special nodal arrangement can be used to approximate multivariate functions (see Fig. 1).

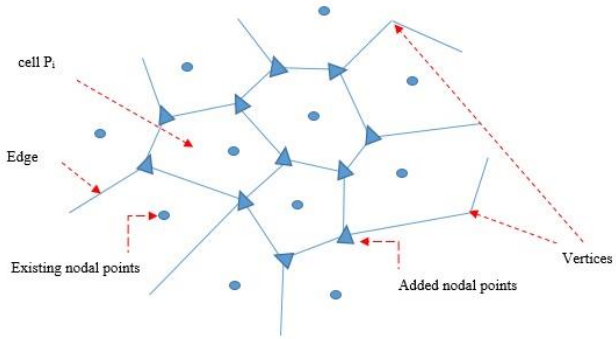

Fig.1
The Voronoi Diagram in the distribution of nodal points.

The Voronoi cells identify nodal points neighboring the desired nodal point by using Delaunay triangulation**.** In such a way that, after the Voronoi celling and its mesh-gridding by the Delaunay diagram, we draw the perpendicular bisectors of the connecting lines between the neighboring nodal points and new points are obtained from their intersection. From connecting these nodal points together, new convex shapes are drawn that create new Voronoi cells for new points added to the analysis domain (see Fig. 2).

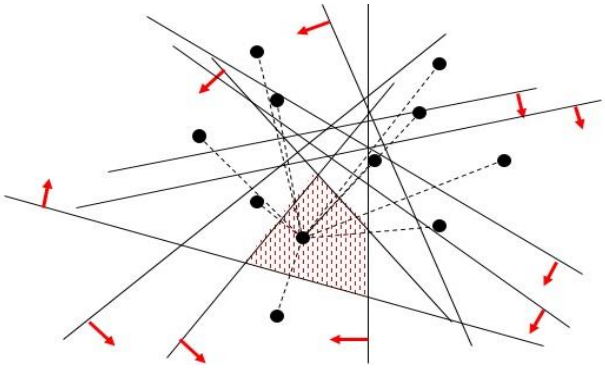

Fig.2
Creation of nodal points and new convex shapes based on the Voronoi Diagram method.

This method can be used as an algorithm to increase the distribution of nodal points to analyze displacement fields and calculate its approximation function in computational fracture mechanics. Usually, the regular distribution of nodal points are used in modeling numerical methods. But in the sections with geometric discontinuity and cracks, in order to increase the accuracy of calculations, the density of nodes increases with a certain order (Of course, irregular or random distribution of nodal points has also been used).

The use of this method (Voronoi Diagram in the distribution of nodal points) means using a kind of Computational Geometry in adding nodal points with known data among the nodal points, in addition to increasing the speed of calculations, it can lead to use the optimal number of the nodal points. In order to increase the efficiency, at each stage after running the VD and adding new nodal points, the error caused by the new arrangement of nodal points is calculated, then in the areas where more errors are reported, other points are calculated by re-running of the VD, added to reduce the error. The calculated error for each node is:

$$e_i = \sqrt{\frac{I_i}{U^T U}} \tag{20}$$

where the nodal functional " I_i " is:

$$I_i = (R_\Omega^T R_\Omega)_i + \alpha_P (R_\Gamma^T R_\Gamma)_i \tag{21}$$

And the residual of the estimation function of the equilibrium equations governing the analysis is:

$$(R_\Omega)_i = (2G\varepsilon_{ij} + \lambda \varepsilon_{kk} \delta_{ij})_i + b_i \quad \text{and} \quad \varepsilon_{ij} = \frac{1}{2}(u_{i,j} + u_{j,i}) \tag{22}$$

Also, the residual of the estimation function resulting from applying the boundary conditions governing the analysis is:

$$(R_\Gamma)_i = \mathbf{D}u_i - \overline{u_I} \tag{23}$$

Finally the total error is calculated from the following relationship:

$$e_{tot} = \sum_{i=1}^{n} e_i \tag{24}$$

5 SHAFT MODELING AND MODE -I STRESS INTENSITY FACTORS

The shaft (general domain) with the geometric specifications presented in Fig. 3, is divided into two parts (cracked area and non-cracked area) for modeling (by using MATLAB software program) in meshless method.

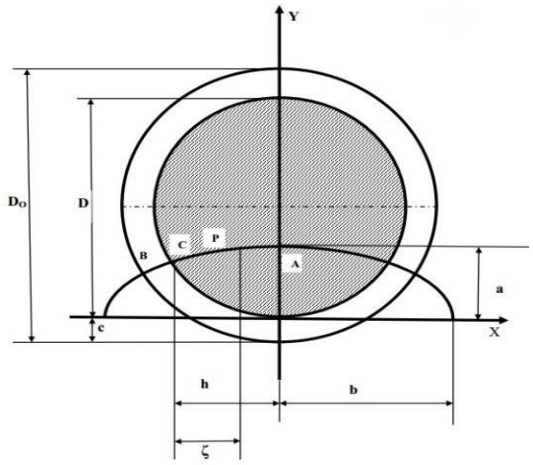

Fig.3
Crack shaft's cross section's geometric characteristics [34].

In Fig. 3, "D_o", "D" , "a" and "b" refers to shaft outer diameter, inner diameter (notched cross section), along the minor and major diameters of semi initial elliptical surface crack, also " h " , "$\xi = \frac{a}{D}$" and "$\zeta^* = \frac{\zeta}{h}$" are the projected length of half of the crack line on its major diameter, relative depth and dimensionless relative depth of the points on the crack line (edge). Point "A" is the deepest point on the crack line and "C", "B" are the edge points of the crack line at the cross-sectional area of the notched and un-notched [34].

The crack area is also divided into two areas, the crack tunnel (Sub-Local domain) and around the crack tunnel (Local domain).Therefore, in the general domain, the regular distribution of nodal points will be used, and in the local domain, as the crack area approaches, the density and number of nodal points will gradually and regularly increase. For this purpose, the Voronoi Diagram technique is used several times. To calculate integral equations, the extruded volumes around the nodal points must have a good overlap (see Fig. 4). Then the nodal points in the crack tunnel (crack line) are considered as analysis points in the geometrical space and domain analysis.

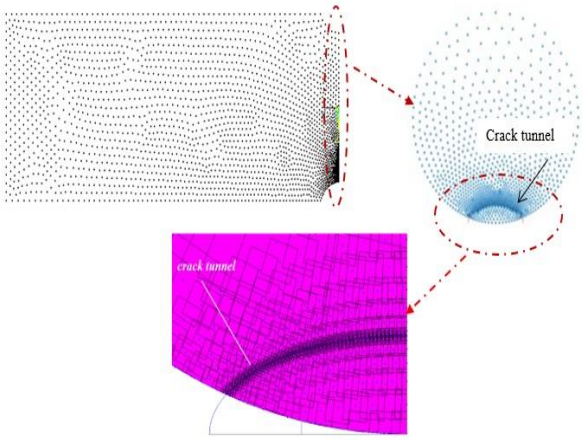

Fig.4
Distribution of nodal points and boundary overlap of extruded volumes around nodal points on the cracked shaft.

The values of 3D-dimensionless Stress Intensity Factors (SIFs) in Mode-I in terms of displacements are:

$$K^{*}_{I,a}=\frac{2G}{\sigma_a(1+k)}\sqrt{\frac{2}{ar}}|\Delta v| \quad for\ tensile\ loading$$
$$K^{*}_{I,b}=\frac{2G}{\sigma_b(1+k)}\sqrt{\frac{2}{ar}}|\Delta v| \quad for\ bending\ loading \tag{25}$$

In Eq. (25), "Δv" is the difference in displacements of the two opposite cross points in planes perpendicular to the crack surface at a distant "r" from the crack edge in the direction of x-axis [36]. Also, "σ_a", "σ_b" and "a" are the tensile stress, the bending stress and the crack depth, respectively.

6 DISCUSSION OF NUMERICAL RESULTS

In order to compare the numerical results deduced from MATLAB software program with those of Ref. [34], the estimated 3D-dimensionless Stress Intensity Factors (3D-SIFs)for the points of the crack front on Un-Notched shaft have been listed in Table 1, based on the relative depth of the crack in tensile or bending cyclic loading in the meshless methods, finite element method and experimental findings.

Table 1
3D- SIFs at different points in the crack line of the Un-Notched cracked shaft under tensile and bending cyclic load.

	Method	ζ^*									
		0.1	0.2	0.3	0.4	0.5	0.6	0.7	0.8	0.9	1.0
Tensile Cyclic	Experimental [34]	1.332	1.289	1.258	1.235	1.219	1.202	1.194	1.188	1.185	1.187
	FEM[34]	1.402	1.357	1.323	1.299	1.283	1.265	1.256	1.249	1.247	1.246
	MLPG-Direct	1.626	1.573	1.534	1.507	1.488	1.467	1.456	1.449	1.446	1.445
Bending Cyclic	Experimental [34]	0.771	0.7251	0.733	0.721	0.712	0.703	0.698	0.695	0.694	0.686
	FEM[34]	0.796	0.781	0.771	0.758	0.749	0.739	0.734	0.731	0.729	0.721
	MLPG-Direct	0.924	0.895	0.873	0.858	0.848	0.837	0.831	0.828	0.826	0.817

Table 1, show that the dimensional stress intensity factors calculated from the MLPG-Direct meshless method are close to the results of Finite Element method. But they are far from experimental results. Now, in order to increase the accuracy of the calculations for finding the optimal value of the Penalty Factor Coefficient "$\beta = 0.0075$" in MLPG used implementing the Mono-objective Particle Swarm Optimization (PSO) algorithm (see Fig. 5).

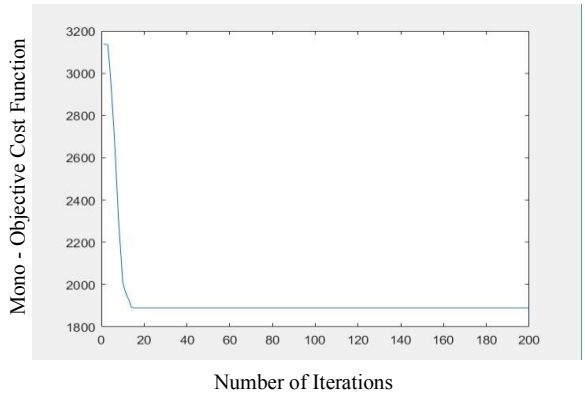

Fig.5
Mono-objective cost function convergence graph in terms of number of iteration in PSO algorithm.

Also, by performing three consecutive stages of the Voronoi diagram method, the optimal arrangement of the nodal points on the crack plane was found (see Fig. 6).

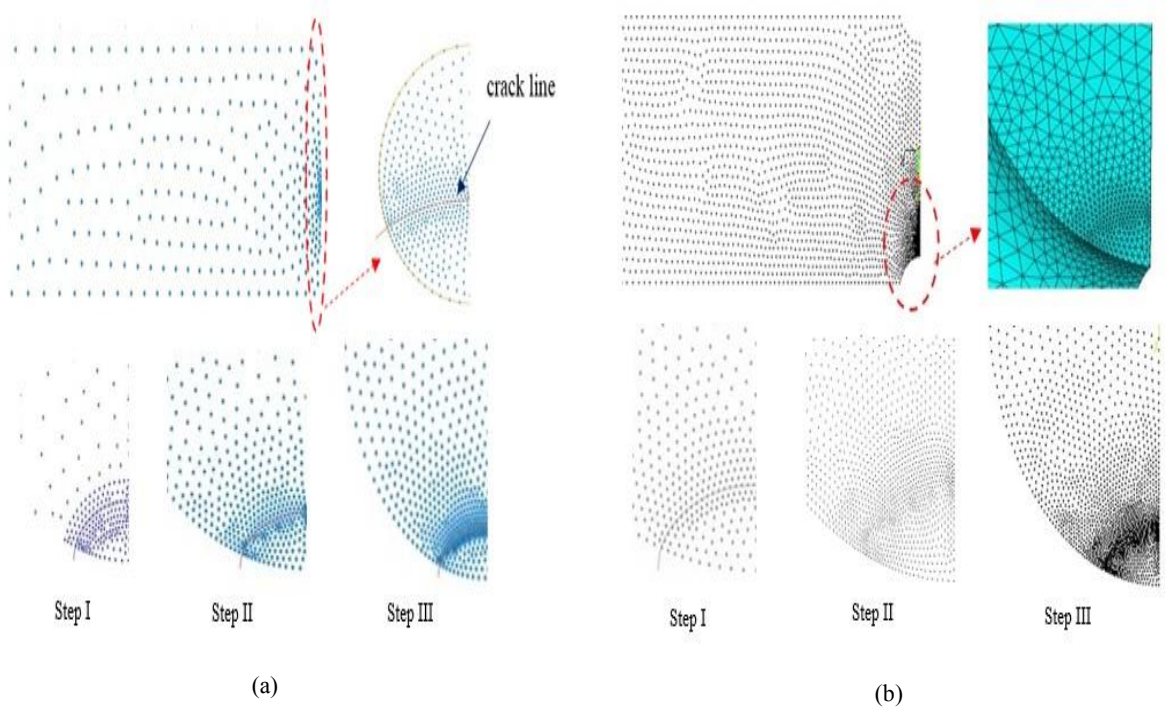

(a) (b)

Fig.6
The three-Step Voronoi Diagram method execution to find the optimal arrangement of nodal points on the crack plane. a) Un-Notched cracked shaft. b) Notched cracked shaft.

The reason for the reduction of the error in the second and third stages is that, at the end of the first and second stage, the VD technique was implemented only in the cells where the error was higher and the nodal points in those cells were increased.

In this way, after three steps of increasing nodal points in the sub- local domain and local domain, the desired nodal arrangement was achieved (see Table 2).

The implementation of this step-by-step computational geometry technique prevents the increase of nodal points and computational cost.

Table 2
The number of nodal points distributed on the crack plane in different steps of the Voronoi technique.

	Step Number	number of nodal points	Total Error
Un-Notched Cracked Shaft	Step I	3739	0.0084
	Step II	6010	0.0038
	Step III	7952	0.00068
Notched Cracked Shaft	Step I	4060	0.0072
	Step II	5969	0.0013
	Step III	6106	0.00041

According to the nodal point arrangement found (VD technique) to use the MLS approximation in the application of the MLPG method with Extended-Enriched-BFs (V-MLS in E-MLPG),the 3D-SIFs in Mode-I for the Un-Notched cracked shaft under tensile and bending cyclic loading will be calculated as Table 3.

For a better comparison and to determine the effectiveness of the method studied in this research (V-MLS in E-MLPG Meshless Method; V-E-MLPG), the FEM numerical method is Extended (FEM is upgraded to XFEM [37]).

The 3D-SIFs found in Table (3), show that the results of XFEM and MLPG-Step-III methods are closer to experimental results compared to other methods.

Now, the effect of the number of sentences of BFs in Khayyam-Pascal's pyramid "N_s" (see Eq. (2)), on the accuracy of calculation of the 3D-SIFs at different points in the crack line of the Un-Notched cracked shaft under tensile and bending cyclic loading will also be investigated Table 4.

Table 3
3D- SIFs at different points in the crack line of the Un-Notched cracked shaft under tensile and bending cyclic load by V- E-MLPG (N_s=4, $\beta = 0.0075$).

	Method	ζ^*									
		0.1	0.2	0.3	0.4	0.5	0.6	0.7	0.8	0.9	1.0
Tensile Cyclic	Experimental [34]	1.332	1.289	1.258	1.2351	1.219	1.202	1.194	1.188	1.185	1.187
	FEM[34]	1.402	1.357	1.323	1.2995	1.283	1.265	1.256	1.249	1.247	1.246
	XFEM	1.324	1.281	1.249	1.2272	1.212	1.195	1.186	1.180	1.178	1.177
	MLPG-Direct	1.626	1.573	1.534	1.5069	1.488	1.467	1.456	1.449	1.446	1.445
	MLPG- Step I	1.493	1.441	1.408	1.3832	1.366	1.347	1.337	1.330	1.327	1.327
	MLPG- Step II	1.373	1.326	1.295	1.2725	1.257	1.239	1.229	1.224	1.221	1.220
	MLPG- Step III	1.336	1.289	1.260	1.2379	1.222	1.205	1.196	1.190	1.188	1.187
Bending Cyclic	Experimental [34]	0.771	0.725	0.733	0.7206	0.712	0.703	0.698	0.695	0.694	0.686
	FEM[34]	0.796	0.781	0.771	0.7582	0.749	0.739	0.734	0.731	0.729	0.721
	XFEM	0.752	0.738	0.728	0.7160	0.708	0.698	0.694	0.691	0.689	0.681
	MLPG-Direct	0.924	0.895	0.873	0.8582	0.848	0.837	0.831	0.828	0.826	0.817
	MLPG- Step I	0.848	0.821	0.801	0.7874	0.779	0.768	0.763	0.759	0.758	0.749
	MLPG- Step II	0.797	0.772	0.753	0.7401	0.732	0.722	0.717	0.714	0.713	0.705
	MLPG- Step III	0.763	0.739	0.721	0.7086	0.701	0.691	0.687	0.684	0.682	0.675

Table 4
The effect of the number of base function sentences on the accuracy of V-E-MLPG method to calculations of 3D-SIFs in the crack line of the Un-Notched cracked shaft.

	Method	ζ^*									
		0.1	0.2	0.3	0.4	0.5	0.6	0.7	0.8	0.9	1.0
Tensile Cyclic	Experimental [34]	1.332	1.289	1.258	1.235	1.219	1.202	1.194	1.188	1.185	1.187
	XFEM	1.324	1.281	1.249	1.227	1.212	1.195	1.186	1.180	1.178	1.177
	MLPG-Step III(N_s=4)	1.336	1.289	1.260	1.238	1.222	1.205	1.196	1.190	1.188	1.187
	MLPG-Step III(N_s=7)	1.335	1.288	1.259	1.237	1.221	1.204	1.195	1.189	1.186	1.186
	MLPG-StepIII(N_s=10)	1.309	1.264	1.235	1.213	1.198	1.181	1.172	1.167	1.164	1.164
Bending Cyclic	Experimental [34]	0.771	0.725	0.733	0.721	0.712	0.703	0.698	0.695	0.694	0.686
	XFEM	0.752	0.738	0.728	0.716	0.708	0.698	0.694	0.691	0.689	0.681
	MLPG-Step III(N_s=4)	0.763	0.739	0.721	0.709	0.701	0.691	0.687	0.684	0.682	0.675
	MLPG-Step III(N_s=7)	0.776	0.752	0.734	0.721	0.713	0.703	0.698	0.695	0.694	0.686
	MLPG-StepIII(N_s=10)	0.787	0.762	0.744	0.731	0.723	0.713	0.708	0.705	0.704	0.696

Convergence Test of 3D- dimensionless SIFs based on the number of nodal points in the crack plane of un-notched shaft under uniaxial cyclic load is presented in Fig. 7.

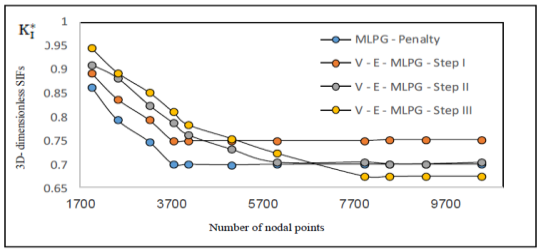

Fig.7
Convergence test (N_s=4 and $\beta = 0.0075$).

In this diagram to finding the suitable number of nodal points and the optimal nodal arrangement, the convergence of V- E -MLPG method with linear-BFs and N_s=4 (see Eq. (2) and Eq. (10)) is drawn during the three steps of the Voronoi Diagram implementation.

The graphs in Fig. 7 indicate the convergence with lower ratio values of 3D-SIFs in the third-step of the implementation of the VD's geometric-computational algorithm.

The effectiveness of calculating 3D-SIFs according to the change "N_s" used in the PBFs can be seen in the graphs drawn in Fig. 8.

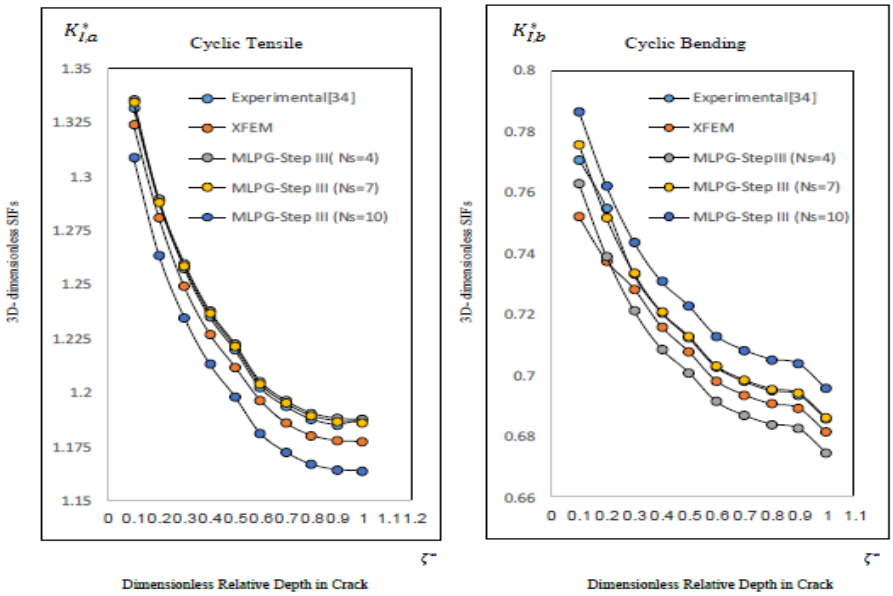

Fig.8

Variations of the 3D-dimensionless SIFs in term of ς^* in an Un-Notched cracked shaft under tensile and bending cyclic load With N_s=4,7,10.

The drawn diagrams in Fig. 8 show that, although the size of the matrix of coefficients and the volume of calculations increases with the increase of the sentences of the PBFs, but it becomes more favorable answers. This is especially evident in the case of bending loading with N_s=7.Approximation with N_s=10 takes more time than N_s=7, but its answers are not cost-effective due to the higher volume of calculations.

In order to examine the effect of increasing the number of sentences of the base function in the third-step of the VD execution on the convergence of the V-E-MLPG method, the diagrams in Fig. 9 have been drawn.

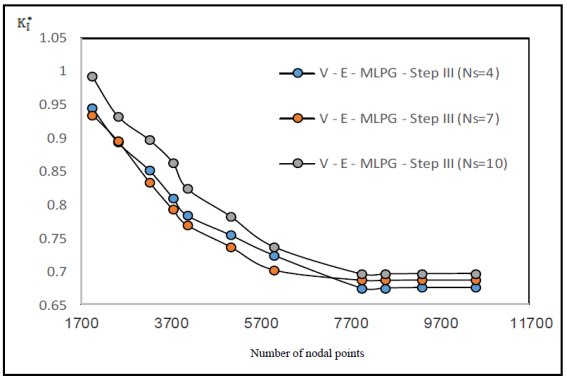

Fig.9

Convergence test in step III (N_s=4,7,10 and $\beta = 0.0075$).

According to the desirability of the answers (see Fig. 7 and Fig8), convergence with relatively lower values of 3D-SIFs (see Fig. 9), the number of suitable sentences to define the base function with N_s=7 was recognized.

For a notched shaft with a semi-elliptical surface crack, the 3D-SIFs by V-E-MLPG Meshless method under Uni-axial loading are according to Table 5.

Table 5
3D-SIFs in the crack line of the Notched cracked shaft by V-E-MLPG method under tensile and bending cyclic load.

	Method	ζ^*									
		0.1	0.2	0.3	0.4	0.5	0.6	0.7	0.8	0.9	1.0
Tensile Cyclic	FEM[34]	1.5804	1.5305	1.4908	1.4645	1.4463	1.4256	1.4153	1.4083	1.4054	1.4047
	XFEM	1.4925	1.4454	1.4078	1.3830	1.3660	1.3463	1.3366	1.3299	1.3272	1.3265
	MLPG- Step III (N_s=4)	1.4488	1.4018	1.3667	1.3426	1.3258	1.3069	1.2974	1.2910	1.2883	1.2877
	MLPG- Step III (N_s=7)	1.5507	1.5004	1.4629	1.4371	1.4191	1.3989	1.3887	1.3818	1.3789	1.3783
	MLPG- Step III (N_s=10)	1.4546	1.4074	1.3721	1.3479	1.3311	1.3121	1.3026	1.2961	1.2934	1.2928
Bending Cyclic	FEM[34]	0.8999	0.8853	0.8716	0.8567	0.8468	0.8354	0.8298	0.9263	0.8246	0.8152
	XFEM	0.8500	0.8362	0.8232	0.8092	0.7998	0.7891	0.7838	0.7805	0.7789	0.7700
	MLPG- Step III (N_s=4)	0.8574	0.8306	0.8106	0.7968	0.7875	0.7722	0.7720	0.7684	0.7613	0.7581
	MLPG- Step III (N_s=7)	0.8719	0.8447	0.8243	0.8103	0.8001	0.7853	0.7851	0.7814	0.7742	0.7709
	MLPG- Step III (N_s=10)	0.8841	0.8565	0.8359	0.8217	0.8121	0.7963	0.7961	0.7924	0.7851	0.7817

In order to be able to compare the results of the V- E – MLPG (Step III with N_s=7) numerical meshless method with the MQ – RPIM meshless method (With optimized values of the shape parameters and the size of the support domain by Multi -Objective PSO optimization algorithm)under the same loading and geometric conditions, the Curves in Fig.(10) are drawn.

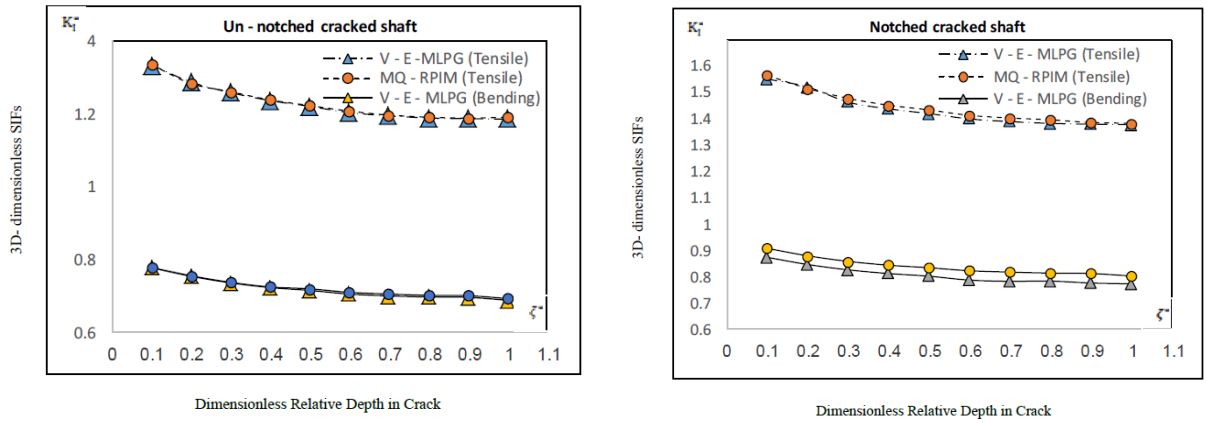

Fig.10
Comparison of the numerical results of calculation (for 3D-SIFs) of two Improved of the extended-enriched meshless methods (V -E -MLPG & MQ – RPIM) in the same loading and geometric conditions. a)Un- notched cracked shaft . b) Notched cracked shaft.

The curves of Fig. 10 show that performing Mono-objective PSO and the implementation of the computational geometry technique of node point distribution for MLPG meshless method and using Multi-objective PSO optimization algorithms in MQ-RPIM meshless method, leads to the closeness of the answers of both methods.

7 CONCLUSION

In this research, to improve the accuracy of calculations in MLPG meshless method with MLS approximation to solving 3D-Linear elasticity and fracture mechanics problems, Mono-objective Particle Swarm Optimization (PSO) algorithm to find the Penalty Factor Coefficient $\beta = 0.0075$ and the Voronoi Diagram (VD) and Delaunay triangulation as a computational geometry technique has been used to optimally distribute nodal points in sub-domains(Crack line and around it on the crack plane). Carrying out this process of computational geometry showed that in order to avoid the arbitrary increase of nodal points in the analysis sub-domain, it is better calculations based on nodal data are performed and the error is checked. Then in the cells with more errors, the nodal points are again increased by running the VD. This operation prevents from increasing the size of the matrix of unknown coefficients and the cost of their calculations. Although the increase in the number of linear and second-order PBFs sentences extracted from Khayyam-Pascal's pyramid (Ns =4,7,10) to define PBF caused; the size matrices of unknown coefficients, the volume and cost of calculations increased. But performing the convergence test and comparing the answers found to calculate the 3D-SIFs in mode-I for a structure with a cracked geometric discontinuity such as a cracked shaft under Uni-axial cyclic loading, with the results of the FEM & XFEM methods, MLPG-Penalty with Ns=4 and Experimental results showed that the accuracy of the calculations of V-E-MLPG, especially for Ns=7 in Step III (after three reruns of VD) have improved significantly.

ACKNOWLEDGMENTS

The authors reserve their utmost gratitude from the Advanced Computing Center of Islamic Azad University Ahvaz Branch for their effective collaborate.

REFERENCES

[1] Belytschko T., Krongauz Y., Organ D., Fleming M., Krysl P., 1996, Meshless methods: an overview andrecent developments, Computer Methods Inapplied Mechanics and Engineering **139**(1-4): 3-47.

[2] Liu G.R., Gu Y.T., 2005, *An Introduction to Meshfree Methods and Their Programming*, Springer Science & Business Media.

[3] Li Q., Shen S., Han Z.D., Atluri S.N., 2003, Application of meshless local Petrov-Galerkin (MLPG) to problems with singularities and material discontinuities in 3-D elasticity, *Computer Modeling in Engineering and Sciences* **4**(5): 571-586.

[4] Han Z.D., Atluri S.N., 2004, Meshless local Petrov-Galerkin (MLPG) approaches for solving 3D problems in elasto-statics, *Computer Modeling in Engineering and Sciences* **6**: 169-188.

[5] Wen P.H., Aliabadi M.H., 2009, Evaluation of mixed-mode stress intensity factors by the mesh-free Galerkin method: static and dynamic, *The Journal of Strain Analysis for Engineering Design* **44**(4): 273-286.

[6] Liu G.R., GuY., 2001, A point interpolation method for two-dimensional solids, *International Journal for Numerical Methods in Engineering* **50**(4): 937-951.

[7] Wang J.G., Liu G., 2002, A point interpolation meshless method based on radial basis functions, *International Journal for Numerical Methods in Engineering* **54**(11): 1623-1648.

[8] Zhuang X., 2010, *Meshless Methods: Theory and Application in 3D Fracture Modelling with Level Sets*, Doctoral Dissertation, Durham University.

[9] Gu Y., Wang W., Zhang L.C., Feng X.Q., 2011, An enriched radial point interpolation method (e-RPIM) for analysis of crack tip fields, *Engineering Fracture Mechanics* **78**(1): 175-190.

[10] Arzani H., Afshar M.H., 2006, Solving Poisson's equations by the discrete least square meshless method, *Transactions on Modelling and Simulation* **42**: 23-31.

[11] Firoozjaee A.R., Afshar M.H., 2009, Discrete least squares meshless method with sampling points for the solution of elliptic partial differential equations, *Engineering Analysis with Boundary Elements* **33**(1):83-92.

[12] Shobeyri G., Afshar M.H., 2010, Simulating free surface problems using discrete least squares meshless method, *Computers & Fluids* **39**(3): 461-470.

[13] Lancaster P., Salkauskas K., 1981, Surfaces generated by moving least squares methods, *Mathematics of Computation* **37**(155): 141-158.

[14] Long S., Hu D., 2003, A study on the weight function of the moving least square approximation in the local boundary integral equation method, *Acta Mechanica Solida Sinica* **3**(16): 276-282.

[15] Yu-ying Y., Jing L., 2005, A study of weight function in element-free Galerkin method, *Journal of Plasticity Engineering* **12**(4): 5-9.

[16] Xu T., Zou P., Xu T., Jiye C., 2010, Study on weight function of meshless method based on B-spline wavelet function, *Third International Joint Conference on Computational Science and Optimization* **1**: 36-40.
[17] Wang Y., Luo Z., Zhang N., 2012, Topology optimization using a radial point-based interpolation method, *International Conference on Computational Methods University of Queensland*.
[18] Zhuang X., Cai Y., Augarde C., 2014, A meshless sub-region radial point interpolation method for accurate calculation of crack tip fields,*Theoretical and Applied Fracture Mechanics* **69**: 118-125.
[19] Shojaei A., Zaccariotto M., Galvanetto U., 2017, Coupling of 2D discretized Peridynamics with a meshless method based on classical elasticity using switching of nodal behavior, *Engineering Computations* **34**(5): 1334-1366.
[20] Karamanli A., 2020, Radial basis Taylor series method and its applications, *Engineering Computations* **38**(5): 2354-2393.
[21] Liu G.R., 2009, *Meshfree Methods: Moving Beyond the Finite Element Method*, CRC press.
[22] Krysl P., Belytschko T., 1997, Element-free Galerkin,method: Convergence of the continuous and discontinuous shape functions, *Computer Methods in Applied Mechanics and Engineering* **148**(3-4): 257-277.
[23] Wang J.G., Liu G., 2002, On the optimal shape parameters of radial basis functions used for 2-D meshless methods, *Computer Methods in Applied Mechanics and Engineering* **191**(23-24): 2611-2630.
[24] Wenterodt C., Von Estorff O., 2009, Dispersion analysis of the meshfree radial point interpolation method for the Helmholtz equation, *International Journal for Numerical Methods in Engineering* **77**(12): 1670-1689.
[25] Sánchez J.M.M., Gonçalves P.B., 2010, Shape function object modeling for meshfree methods, *Mecánica Computacional* **29**(47): 4753-4767.
[26] Razmjoo H., Movahhedi M., Hakimi A., 2010, An efficient meshless method based on a new shape function, *International Journal of Numerical Modelling: Electronic Networks, Devices and Fields* **23**(6): 503-521.
[27] Afsari A., Movahhedi M., 2013,Criterion for selecting the shape functions in electromagnetic meshless methods, *IET Science, Measurement & Technology* **7**(3): 157-165.
[28] Bozkurt O.Y., Kanber B., AŞIK M.Z., 2013, Assessment of RPIM shape parameters for solution accuracy of 2D geometrically nonlinear problems, *International Journal of Computational Methods* **10**(03): 1350003.
[29] Moussaoui A., Bouziane T., 2016, Numerical study of the shape parameter dependence of the local radial point interpolation method in linear elasticity, *MethodsX* **3**: 178-187.
[30] Ghaffarzadeh H., Barghian M., Mansouri A., Sadeghi M., 2016, Study on meshfree hermite radial point interpolation method for flexural wave propagation modeling and damage quantification, *Latin American Journal of Solids and Structures* **13**: 2606-2627.
[31] Shivanian E., 2020, Formulation of pseudospectral meshless radial point Hermit interpolation for the Motz problem and comparison to pseudospectral meshless radial point interpolation, *Multidiscipline Modeling in Materials and Structures* **16**(1): 1-20.
[32] Li Y., Liu G.R., 2019, An element-free smoothed radial point interpolation method (EFS-RPIM) for 2D and 3D solid mechanics problems, *Computers & Mathematics with Applications* **77**(2): 441-465.
[33] Ariannezhad B., Shahrooi S., Shishehsaz M., 2022,On applicability of MQ-RPIM and MLPG meshless methods with 3D extended-enriched base functions for estimation of mode I stress intensity factor and fatigue crack growth in cyclic tensile and bending load of an un-notched and notched shaft, *The Journal of Strain Analysis for Engineering Design* **57**(5): 340-359.
[34] Carpinteri A., Brighenti R., Vantadori S., 2006, Surface cracks in notched round bars under cyclic tension and bending, *International Journal of Fatigue* **28**(3): 251-260.
[35] Hosseini Sh., Soltani B., 2017, Analysis of rectangular stiffness plates based on fstd and meshless collection method, *Journal of Solid Mechanics* **9**(3): 568-586.
[36] Eskandari H., Ghanbari M., Mirzadeh F., 2021, Three-dimensional stress analysis for semi-elliptical cracks in the connection of cylinder-hemispherical head for thick-walled cylindrical pressure vessels, *Journal of Solid Mechanics* **13**(1): 1-10.
[37] Sharma K., 2014, Crack interaction studies using XFEM technique, *Journal of Solid Mechanics* **6**(4): 410-421.